Macromolecular Rapid Communications
www.mrc-journal.de

Dye-Loaded Mechanochromic and pH-Responsive Elastomeric Opal Films

*Tamara Winter, Anna Boehm, Volker Presser, and Markus Gallei**

In this work, the preparation and fabrication of elastomeric opal films revealing reversible mechanochromic and pH-responsive features are reported. The core–interlayer–shell (CIS) particles are synthesized via stepwise emulsion polymerization leading to hard core (polystyrene), crosslinked interlayer (poly(methyl methacrylate-*co*-allyl methacrylate), and soft poly(ethyl acrylate-*co*-butyl acrylate-*co*-(2-hydroxyethyl) methacrylate) shell particles featuring a size of 294.9 ± 14.8 nm. This particle architecture enables the application of the melt-shear organization technique leading to elastomeric opal films with orange, respectively, green brilliant reflection colors dependent on the angle of view. Moreover, the hydroxyl moieties as part of the particle shell are advantageously used for subsequent thermally induced crosslinking reactions enabling the preparation of reversibly tunable mechanochromic structural colors based on Bragg's law of diffraction. Additionally, the CIS particles can be loaded upon extrusion or chemically by a postfunctionalization strategy with organic dyes implying pH-responsive features. This convenient protocol for preparing multi-responsive, reversibly stretch-tunable opal films is expected to enable a new material family for anti-counterfeiting applications based on external triggers.

Photonic structural materials have received significant attention, and they have been studied and engineered as candidates for display technologies, sensors, and as anti-counterfeiting materials over the last decades.[1–3] The most interesting building block for photonic materials is represented by monodisperse colloids, which can be prepared by an inexpensive and convenient bottom-up process, for instance, by the Stöber process (SiO_2)[4,5] or means of emulsion polymerization (organic and/or hybrid particles). As a result, particle-based films from these materials typically feature iridescent reflection colors caused by Bragg diffraction of visible light.[6–9] Reviews dealing with self-assembled photonic materials and applications thereof are given by Galisteo-López et al.[10] and other authors.[11–14] In general, the mechano-responsiveness in soft materials attracted tremendous attention for various sensing applications in the past.[15–19] So-called elastomeric polymer opals consist of well-defined (concerning size and form) particles with diameters typically in the range of 200–350 nm embedded in a soft matrix. Such particle-based films can be fabricated to prepare reversibly stretch-tunable materials showing remarkable color changes due to a variation of the 111 (200) plane spacing of the colloidal crystal structure.[20–22] The distance between the underlying spheres can also be triggered and modulated by external triggers such as organic solvents, pH value, light, magnetic field or combinations thereof.[23–29] Advances in the field of stimuli-responsive opal materials have been reviewed,[30,31] while very recently Chen and Hong reported on the mechanochromism of structural-colored materials.[32] In general, the lack of mechanical strength in soft polymer-based opal films and hydrogels can be overcome by subsequent crosslinking strategies of the soft matrix after the film preparation. As a result, excellent optical performance can be combined with a fully reversible mechanochromic behavior[33–35] after the particles' precise arrangement in such elastomeric opal films by combinations of melting and shear-ordering methods.[14,36–38] Current invisible photonic crystal patterns have been developed successfully to allow images to appear in several different ways, such as selective chemical wetting,[39] magnetic field manipulation,[40] and mechanical stretching.[41–43] With the scalable fabrication of these stimuli-responsive photonic crystals, such materials are well suited for application in chemical sensing and anti-counterfeiting devices, for document authentication, secret information encoding, and a variety of other opportunities.

T. Winter
Ernst-Berl-Institute of Chemical Engineering and Macromolecular Chemistry
Technische Universität Darmstadt
Alarich-Weiss-Straße 4, Darmstadt 64287, Germany
T. Winter, Prof. V. Presser
Department of Materials Science and Engineering
Saarland University
Campus D2 2, Saarbrücken 66123, Germany
A. Boehm, Prof. M. Gallei
Chair in Polymer Chemistry
Saarland University
Campus Saarbrücken C4 2, Saarbrücken 66123, Germany
E-mail: markus.gallei@uni-saarland.de
Prof. V. Presser
INM – Leibniz-Institute for New Materials
Campus D2 2, Saarbrücken 66123, Germany
The ORCID identification number(s) for the author(s) of this article can be found under https://doi.org/10.1002/marc.202000557.

DOI: 10.1002/marc.202000557

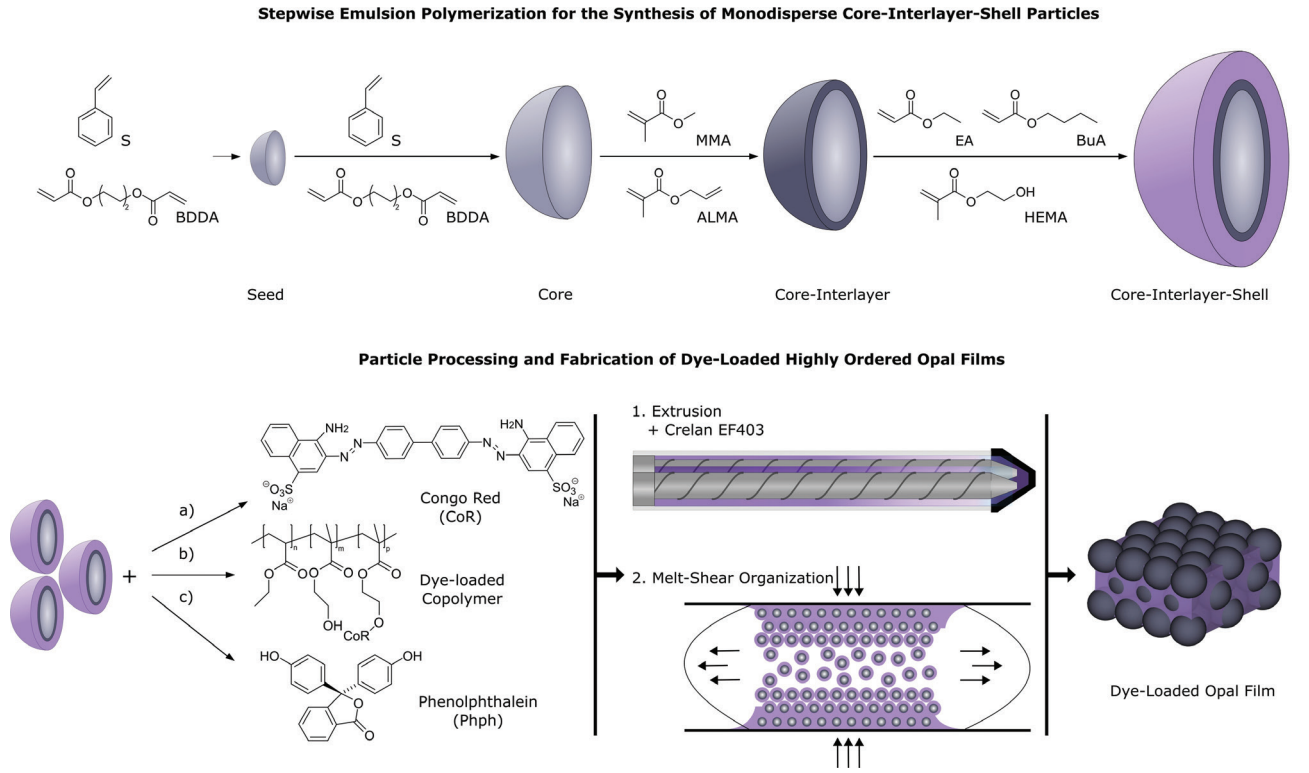

Scheme 1. Top: Stepwise synthesis of elastomeric core–interlayer–shell (CIS) particles via starved-feed emulsion polymerization (see text). Bottom: Particle dye loading with different reagents a) pure congo red, b) poly(styrene-*co*-2-(hydroxyethyl) methacrylate) (P(S-*co*-HEMA)) functionalized with congo red, and c) pure phenolphthalein and homogenization. This is followed by a melt-shear organization of the CIS particles to generate a dye-loaded opal film.

In the present study, we present a convenient approach for combining structurally colored elastomeric opal films featuring pH-responsive dyes as part of the soft opal matrix. The hard core/soft shell particles were designed using starved-feed emulsion polymerization, which was tailored for: i) the convenient melt-shear organization, that is, shear-induced ordering of the particles, ii) subsequent thermally induced crosslinking strategies for gaining access to mechanochromic features, and finally, iii) the incorporation of organic dyes or dye-functionalized copolymers as matrix additives. The optical properties were investigated upon the application of external triggers such as mechanical stress and pH-responsiveness. These materials are promising for applications related to security and sensing.

For the fabrication of dye-loaded opal films showing mechanochromic properties, core–interlayer–shell (CIS) particles were prepared by seeded and stepwise emulsion polymerization technique (EP) followed by different processing steps illustrated in **Scheme 1**. To synthesize monodisperse particles, the starved-feed mode for emulsion polymerization is mandatory, as this technique can be used for tailoring the particle shape and size distribution without any secondary particle nucleation. In the first step, pristine crosslinked poly(styrene-*co*-butanediol diacrylate) (P(S-*co*-BDDA)) seeds were synthesized using a batch process followed by the continuous addition of either S and BDDA to obtain hard core particles. We controlled the surfactant amount in the batch process and the monomer content during the starved-feed mode. Thereby, the core particles' average diameter was adjusted to be 203.2 ± 7.8 nm (according to dynamic light scattering (DLS) data). Thus, permitting final opal films' preparation shows a reflection color in the range of the visible light. Bragg's law of diffraction considers both the size of the particles and the effective refractive index contrast. Crosslinking of the PS cores is needed to avoid particle deformation during extrusion and the melt-shear organization at a temperature of 120 °C. Using BDDA as the crosslinker also offers the possibility of reinitiating the polymerization via free vinylic moieties on the particle surface. Thus, the crosslinked interlayer of ≈5 nm containing methyl methacrylate (MMA) and allyl methacrylate (ALMA) was introduced. Based on the two different reactive sites of ALMA, subsequent anchoring of the soft polymer shell material was possible.

Our samples' specific particle architecture is an essential prerequisite for keeping the core particle shape and introducing a soft copolymer shell in the next step. Concerning the generation of opal films featuring reversible mechanochromic properties, the resulting glass transition temperature (T_g) of the corresponding shell material should be below room temperature. At the same time, the polymer's stability should be given by the covalent linkages of the shell material. The effective refractive index contrast between the core and shell material are key factors to enable structural colors. For this purpose, a combination of ethyl acrylate (EA) and *n*-butyl acrylate (BuA) was used due to their low glass transition temperatures[44] of T_g(EA) = −22 °C and T_g(BuA) = −56 °C as well as their relatively low refractive indices of n(EA) = 1.48 and

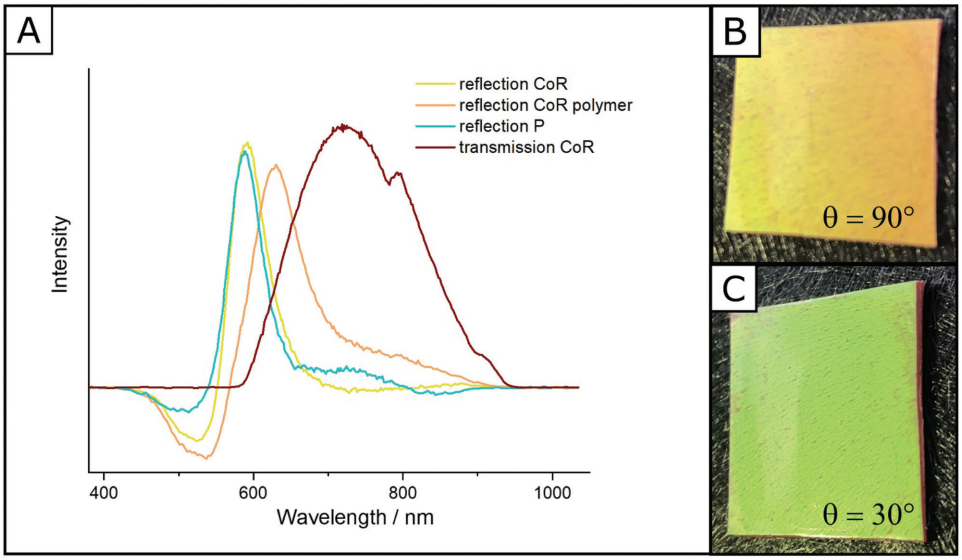

Figure 1. A) UV–vis reflection and transmission spectra of the dye-loaded opal film. B,C) Corresponding photographs from different angles of view.

n(BuA) = 1.47 compared to the PS core particles (n(PS) = 1.59).[45] An additional 2 wt% of 2-(hydroxyethyl) methacrylate (HEMA) providing hydroxylic groups for final thermal crosslinking reactions were introduced into the shell material.

To evaluate the successful preparation of tailored particles with a core–shell architecture, transmission electron microscope (TEM) measurements were carried out after each synthesis step (Figure S2, Supporting Information). From these images, it can be concluded that well-defined CIS particles were prepared starting from 203.2 ± 7.8 nm crosslinked PS cores to 294.9 ± 14.8 nm (both according to DLS data) core–interlayer–shell particles (batch no. 1). The corresponding small standard deviations (<5%) indicate that monodisperse CIS particles were obtained, a key feature for further processing and colloidal self-assembly. By these basic prerequisites, we produced highly ordered 3D opal films after melt-shear organization.

DLS measurements (Figure S3, Supporting Information) of the diluted particle dispersions further confirm these results showing a narrow size distribution as well as an increasing hydrodynamic diameter for the CIS particle synthesis starting from 203.2 ± 7.8 nm crosslinked PS cores to 294.9 ± 14.8 nm CIS particles (299.1 ± 27.3 nm for batch no. 2), which is also proved by the brilliant reflection color of the dried particle dispersion. All obtained data on particle size were in good agreement with theoretical expectations to monomer consumption and polymer yield (see the Experimental Section). The use of two batches is merely attributed to the polymer amount needed to fabricate several opal films. Before the processing experiments, the CIS particles' thermal properties, especially for the shell material, were verified by using differential scanning calorimetry (DSC) measurements to evaluate both the monomer incorporation and tailoring of the processing parameters depending on the glass transition temperature of the shell material. In Figure S4 (Supporting Information), a glass transition temperature of –11.3 °C (–11.4 °C for batch no. 2) for the final material P(S_{91}-*co*-BDDA$_9$)@P(MMA$_{90}$-*co*-ALMA$_{10}$)@P(EA$_{88}$-*co*-BuA$_{10}$-*co*-HEMA$_2$) is shown, making these elastomeric polymer particles suitable for the preparation of reversibly stretchable, soft opal films featuring structural colors.

Before analyzing the full optical properties the CIS material was further processed to incorporate different dyes. The lyophilized pure particle mass was mixed with two different dyes, namely, phenolphthalein (P) and congo red (CoR) as well as with a congo red-functionalized copolymer to obtain a homogeneous and processable material. To the three different core/shell particle masses, a blocked oligo isocyanate crosslinker (Crelan EF403) was added before processing in a micro extruder (Experimental Section).

As illustrated in Scheme 1 (bottom), pure congo red (a), a P(EA-*co*-HEMA) copolymer functionalized with congo red (b), and pure phenolphthalein were selected as dyes. The postfunctionalization of the copolymer with congo red and polymer characterization are described in the Supporting Information. The extrusion strands were subjected to the melt-shear organization technique to prepare the respective dye-loaded opal films. As described in the Introduction, by this method, freestanding photonic crystals were obtained. Within the present study, during the shear-induced self-assembly, the crosslinked PS core particles were arranged into a face-centered cubic lattice surrounded by the dye-loaded soft polymer matrix, which stemmed from the covalently attached shell material, as described in previous literature.[38,46,47] To achieve a reversibly tunable mechanochromic response and simultaneously avoid an inelastic behavior of the obtained opal films upon stretching, the opal films were treated at 190 °C. Thereby, we induced a thermal crosslinking reaction between the PHEMA-containing shell material's hydroxyl moieties and the Crelan EF403. In the congo red-loaded opal films, both the amine moieties of the dye and the hydroxy groups of the dye-functionalized PHEMA copolymer will be capable of covalently immobilizing the dye in the shell-forming polymer chains. As a result, the dye's significant leakage is avoided if desired for the application as anti-counterfeiting material.

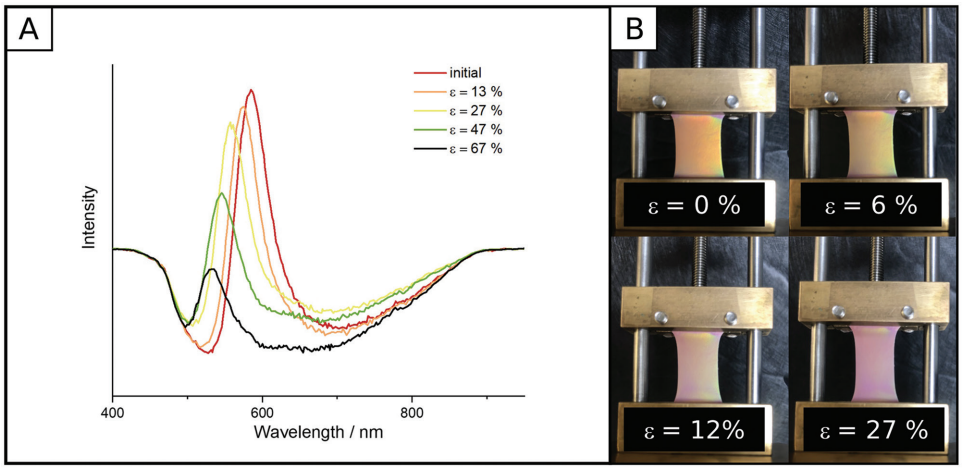

Figure 2. a) Strain-dependent UV–vis reflection spectra of the opal film containing the dye-loaded copolymer of P(EA-*co*-HEMA) and b) corresponding photographs of the opal film while stretching from $\varepsilon = 0\%$ to $\varepsilon = 27\%$.

In the following, we investigate the optical properties of the dye-loaded opal films and the mechanochromic response of the herein produced crosslinked films. All original opal films featured almost the same yellow-orange reflection color, which agrees with the corresponding UV–vis measurements showing a Bragg peak at $\lambda = 588$ nm at an angle of view of 90° (**Figure 1**).

Two different CIS particle batches were synthesized. The particles' hydrodynamic diameter from batch no. 1 is 294.9 ± 14.8 and 299.1 ± 27.3 nm for batch no. 2 (both according to DLS data). The small redshift of the photonic bandgap from 588 to 630 nm belonging to the dye-containing copolymer aligns with the use of two different particle batches. The reflection colors are induced by the surface parallel (111)-lattice planes of hexagonally arranged PS cores embedded in the matrix of P(EA_{88}-*co*-BuA_{10}-*co*-$HEMA_2$) featuring an effective refractive index contrast of $\Delta n \approx 0.12$ between the core ($n_{PS} = 1.59$) and shell ($n_{Copolymer} \approx 1.47$) material. Moreover, the presence of congo red within the opal film was characterized by UV–vis measurements in transmission mode (Figure 1, red curve). To demonstrate the mechanochromic properties, strain-dependent UV–vis measurements were carried out by characterizing the stop-band shift while applying strain up to $\varepsilon = 67\%$.

Figure 2 exemplifies this behavior for the opal film containing the congo red functionalized copolymer of P(EA-*co*-HEMA). All spectra were recorded at an incident angle of 90° in reflection mode using a normal incidence, keeping the light spot constant. Figure 2 shows the reflection spectra and the corresponding photographs from the original opal film compared to the material after stretching.

Furthermore it can be shown that increasing the strain leads to a constant blueshift of the Bragg peak until the reflection color almost wholly disappeared. This behavior can also be seen visually. These results further prove that the intense structural color was more dominant based on the highly ordered particle domains inside the opal film. While stretch-tuning the opal film, the reflection color changed from orange to yellow, over to green, until it disappears (Figure 2B). Moreover, this behavior is fully reversible, and upon relaxation of the opal film to its initial shape, the pristine reflection color could be observed. Detailed combined mechanical and optical characterization after the application of thermally induced crosslinking protocols has been described in a previous study.[35] The other opal film samples, containing pure phenolphthalein and pure congo red, showed a similar optical response, as confirmed by UV–vis data.

Both dyes, congo red and phenolphthalein, could be extracted from the opal film simply by using a sessile drop on top of the film surface. In comparison, opal films featuring the dye-containing copolymer crosslinked inside the opal matrix were not prone to a dye leakage (**Figure 3**). The extraction of phenolphthalein could be observed immediately after setting the water drop on the opal film surface. However, the extraction of congo red was slower, possibly because of the increased sterical hindrance of the molecule and stronger interaction with the film material.

To further investigate the leakage of the dyes, a piece of each opal film (1 cm^2) was inserted into 8 mL of water for at least 15 h. Afterwards, the final dye-loaded water residues were characterized by UV–vis measurements to detect whether the dyes were extracted or stayed inside the opal film under these treatments (Figure S5, Supporting Information). As can be concluded from Figure S5 (Supporting Information), pure phenolphthalein, as well as congo red, could be detected in the water-based residues showing absorption bands at 555 nm (phenolphthalein)[48] and 510 nm (congo red),[49] which is in good agreement with the literature. In contrast, the opal film's residue within the dye-containing copolymer did not show any absorption signal, demonstrating the chemical incorporation of the copolymer inside the opal film matrix. All these observed properties make the materials applicable for different sensor strategies, where the stimuli can either be used separately for a specific kind of safety feature or in combination resulting in a double safety functionality. Furthermore, the mechanochromic behavior of these freestanding opal films can be tailored by several parameters (e.g., core particle size, core–shell ratio, and crosslinking density), and the resulting reflection colors can be controlled. Within the present work, additional features for

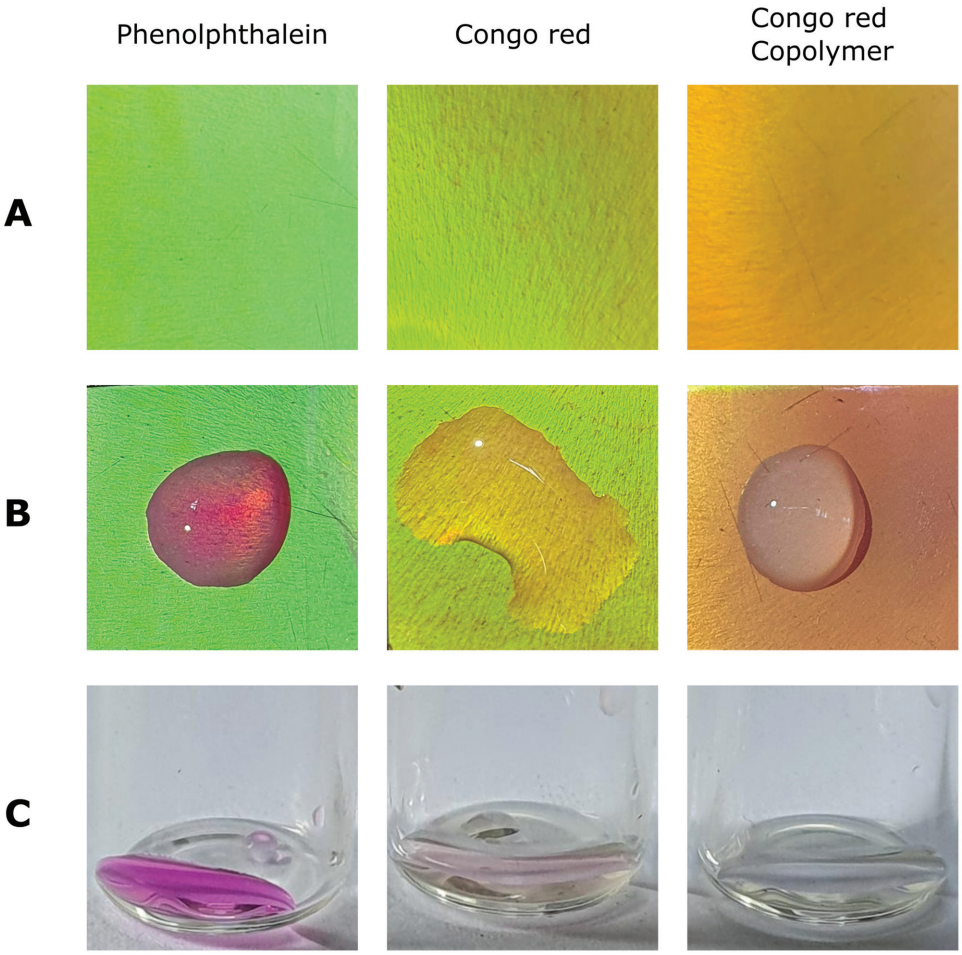

Figure 3. Photographs of the opal films containing three different dyes: A) initial state, B) with a water droplet for extraction (in case of phenolphthalein: pH = 11), and C) water residues after opal film treatment. Cutouts of the opal films shown in (A) and (B) correspond to piece sizes of 1 cm^2.

these elastomeric opal films can be conveniently introduced by incorporating organic dye molecules, which again can feature a pH-responsive performance, interesting for optical sensors or the fabrication of double safety anti-counterfeiting materials.

In conclusion, an efficient protocol for the preparation of anti-counterfeiting materials based on elastomeric opal films featuring mechanochromic properties was demonstrated within this work. Stepwise emulsion polymerization led to monodisperse CIS particles consisting of crosslinked PS cores (d = 203.2 ± 7.8 nm) and a soft shell of P(EA_{88}-*co*-BuA_{10}-*co*-$HEMA_2$). Subsequent processing using extrusion enabled the incorporation of two organic dyes, that is, phenolphthalein and congo red, and a dye-containing copolymer as well as a thermal crosslinker (Crelan EF403). According to Bragg's law of diffraction, we used the melt-shear organization technique and subsequent thermal treatment to prepare elastomeric mechanochromic opal films featuring angle-dependent reflection colors. UV–vis measurements allowed for measuring the evaluation of the strain-induced change of the Bragg peak maximum as well as the detection of the different dyes.

Moreover, the extraction behavior was evaluated by setting a water droplet on the surface of the dye-loaded opal films. The extraction duration of the pure dyes, phenolphthalein, and congo red, depends on the molecule size, polarity and the interaction with the polymer matrix. Thus, the extraction of phenolphthalein was faster than the extraction of congo red. In the case of the dye-loaded copolymer containing opal film, there was no extraction residue since the copolymer is incorporated within the opal film matrix. For that reason, we envision the herein investigated dye-containing and stretchable opal films as promising candidates for anti-counterfeiting and sensing materials.

Experimental Section

Synthesis of PS@P(MMA_{85}-co-$ALMA_{15}$)@P(EA_{88}-co-BuA10-co-$HEMA_2$) CIS Particles: The CIS particles were synthesized starting from the polystyrene (PS) core particle dispersion (particle size 203.2 ± 7.8 nm, synthesis see the Supporting Information) in a 250 mL double-wall reactor with a stirrer and a reflux condenser under a nitrogen atmosphere at 75 °C. For this purpose, 27.39 g of the PS core dispersion and 28.17 g deionized water were filled into the reactor and stirred at 300 rpm. The starved-feed emulsion polymerization was initiated by the addition of 0.006 g sodium disulfite (NaDS), 0.069 g sodium persulfate (NaPS), and 0.006 g NaDS (each component was dissolved in 5 g of deionized water). After 15 min reaction time, a monomer emulsion (ME1) consisting of 0.007 g sodium dodecyl sulfate (SDS), 0.014 g Dowfax 2A1, 0.61 g methyl methacrylate (MMA), 0.068 g allyl methacrylate (ALMA), and 3 g

deionized water was continuously added with a flow rate of 0.3 mL min^{-1} using a rotary piston pump. After the complete addition of ME1 and an additional 20 min stirring at this temperature, the polymerization was reinitiated by adding 0.011 g NaPS. After an additional 10 min, a second monomer emulsion (ME2) containing 0.057 g SDS, 0.046 g Dowfax 2A1, 0.08 g potassium hydroxide (KOH), 12.69 g ethyl acrylate (EA), 1.44 g butyl acrylate (BuA), 0.29 g 2-(hydroxyethyl) methacrylate (HEMA), and 18.8 g deionized water was added continuously with a flow rate of 0.3 mL min^{-1} using a rotary piston pump. After the complete addition of ME2 the reaction was kept at a constant temperature for an additional 45 min, resulting in a solid content of the CIS particle dispersion of 19.24 wt%. The average hydrodynamic diameter of the final CIS particles was 294.9 ± 14.8 nm, determined by DLS. According to the same protocol described above, a second batch (batch no. 2) of PS@P(MMA_{85}-*co*-$ALMA_{15}$)@P(EA_{88}-*co*-BuA_{10}-*co*-$HEMA_2$) was synthesized starting with the same PS core particles, as used before. The average hydrodynamic diameter of the final CIS particles of batch no. 2 was 299.1 ± 27.3 nm, as determined by DLS with a solid content of 12.37 wt%.

Particle Processing and Dye-Loaded Opal Film Preparation: For the preparation of dye-loaded elastomeric PS@P(MMA_{85}-*co*-$ALMA_{15}$)@P(EA_{88}-*co*-BuA_{10}-*co*-$HEMA_2$) opal films, the obtained CIS particles were first lyophilized. In general, three opal films were prepared to contain different kind of dye reagents: a linear P(EA-*co*-HEMA) copolymer postfunctionalized with congo red (dye no. 1) (the polymer was synthesized by free radical polymerization, see the Supporting Information for specifications), pure congo red (dye no. 2), and pure phenolphthalein (P, dye no. 3). For homogenization of the particle mass, 3.22 g of the precursor powder (batch no. 1 was used for dye no. 1 and batch no. 2 for dye no. 2 and no. 3) was mixed with 0.282 g Crelan EF403 and either 100 mg of the different dye reagents in a micro extruder (HAAKE Minilab II 350, Thermo Scientific) at 120 °C and 130 rpm. For opal film formation, a 1.6 g portion of the elastomeric dye-containing polymer mass was covered with two polyethylene terephthalate (PET) foils (Mylar A75, DuPont) and inserted into a Collin laboratory press P 300 E (Dr. Collin, Ebersberg, Germany). During the melt-shear organization, the particle mass was formed into opal discs of ≈4 cm in diameter at 120 °C, 5 bar, and a holding time of 3 min. For subsequent crosslinking reaction, the obtained freestanding opal films were separated from the PET foils and treated in an oven at 190 °C for at least 10 min.

Supporting Information

Supporting Information is available from the Wiley Online Library or from the author.

Acknowledgements

T.W. and A.B. contributed equally to this work. This research was partially supported by the DFG project GA2169/5-1. The authors thank Hanna Hübner for TEM measurements. V.P. thanks Eduard Arzt (INM) for his continued support. Correction added on 5th February 2021, after first online publication: Projekt Deal funding statement has been added.

Open access funding enabled and organized by Projekt DEAL.

Conflict of Interest

The authors declare no conflict of interest.

Keywords

elastomeric opals, functional polymers, photonic crystals, self-assembly, stimuli-responsive materials

Received: September 27, 2020
Revised: October 19, 2020
Published online: November 30, 2020

[1] Y. Xia, B. Gates, Y. Yin, Y. Lu, *Adv. Mater.* **2000**, *12*, 693.
[2] A. P. Hynninen, J. H. Thijssen, E. C. Vermolen, M. Dijkstra, A. van Blaaderen, *Nat. Mater.* **2007**, *6*, 202.
[3] R. D. L. Rue, *Nat. Mater.* **2003**, *2*, 74.
[4] C. Graf, A. V. Blaaderen, *Langmuir* **2002**, *18*, 524.
[5] W. Stöber, A. Fink, E. Bohn, *J. Colloid Interface Sci.* **1968**, *26*, 62.
[6] F. Marlow, Muldarisnur, P. Sharifi, R. Brinkmann, C. Mendive, *Angew. Chem., Int. Ed.* **2009**, *48*, 6212.
[7] A. Stein, F. Li, N. R. Denny, *Chem. Mater.* **2008**, *20*, 649.
[8] A. Vlad, A. Frölich, T. Zebrowski, C. A. Dutu, K. Busch, S. Melinte, M. Wegener, I. Huynen, *Adv. Funct. Mater.* **2013**, *23*, 1164.
[9] G. von Freymann, V. Kitaev, B. V. Lotsch, G. A. Ozin, *Chem. Soc. Rev.* **2013**, *42*, 2528.
[10] J. F. Galisteo-López, M. Ibisate, R. Sapienza, L. S. Froufe-Pérez, Á. Blanco, C. López, *Adv. Mater.* **2011**, *23*, 30.
[11] R. J. Martín-Palma, M. Kolle, *Opt. Laser Technol.* **2019**, *109*, 270.
[12] J. Hou, M. Li, Y. Song, *Nano Today* **2018**, *22*, 132.
[13] E. S. A. Goerlitzer, R. N. K. Taylor, N. Vogel, *Adv. Mater.* **2018**, *30*, 1706654.
[14] M. Gallei, *Macromol. Rapid Commun.* **2018**, *39*, 1700648.
[15] K. Shanmuganathan, J. R. Capadona, S. J. Rowan, C. Weder, *ACS Appl. Mater. Interfaces* **2010**, *2*, 165.
[16] J. R. Kumpfer, S. J. Rowan, *J. Am. Chem. Soc.* **2011**, *133*, 12866.
[17] C. M. Kingsbury, P. A. May, D. A. Davis, S. R. White, J. S. Moore, N. R. Sottos, *J. Mater. Chem.* **2011**, *21*, 8381.
[18] M. M. Caruso, D. A. Davis, Q. Shen, S. A. Odom, N. R. Sottos, S. R. White, J. S. Moore, *Chem. Rev.* **2009**, *109*, 5755.
[19] D. A. Davis, A. Hamilton, J. Yang, L. D. Cremar, D. Van Gough, S. L. Potisek, M. T. Ong, P. V. Braun, T. J. Martinez, S. R. White, J. S. Moore, N. R. Sottos, *Nature* **2009**, *459*, 68.
[20] S. A. Asher, J. Holtz, L. Liu, Z. Wu, *J. Am. Chem. Soc.* **1994**, *116*, 4997.
[21] B. Viel, T. Ruhl, G. P. Hellmann, *Chem. Mater.* **2007**, *19*, 5673.
[22] H. Fudouzi, T. Sawada, *Langmuir* **2006**, *22*, 1365.
[23] L. Duan, B. You, S. Zhou, L. Wu, *J. Mater. Chem.* **2011**, *21*, 687.
[24] H. Jiang, Y. Zhu, C. Chen, J. Shen, H. Bao, L. Peng, X. Yang, C. Li, *New J. Chem.* **2012**, *36*, 1051.
[25] H. Ma, K. Tang, W. Luo, L. Ma, Q. Cui, W. Li, J. Guan, *Nanoscale* **2017**, *9*, 3105.
[26] D. Scheid, C. Lederle, S. Vowinkel, C. G. Schäfer, B. Stühn, M. Gallei, *J. Mater. Chem. C* **2014**, *2*, 2583.
[27] C. G. Schäfer, C. Lederle, K. Zentel, B. Stühn, M. Gallei, *Macromol. Rapid Commun.* **2014**, *35*, 1852.
[28] C. G. Schäfer, M. Gallei, J. T. Zahn, J. Engelhardt, G. P. Hellmann, M. Rehahn, *Chem. Mater.* **2013**, *25*, 2309.
[29] T. Winter, X. Su, T. A. Hatton, M. Gallei, *Macromol. Rapid Commun.* **2018**, *39*, 1800428.
[30] G. Isapour, M. Lattuada, *Adv. Mater.* **2018**, *30*, 1707069.
[31] Y. Takeoka, *J. Mater. Chem. C* **2013**, *1*, 6059.
[32] G. Chen, W. Hong, *Adv. Opt. Mater.* **2020**, *8*, 2000984.
[33] P. Spahn, C. E. Finlayson, W. M. Etah, D. R. E. Snoswell, J. J. Baumberg, G. P. Hellmann, *J. Mater. Chem.* **2011**, *21*, 8893.
[34] A. M. Schlander, M. Gallei, *ACS Appl. Mater. Interfaces* **2019**, *11*, 44764.
[35] C. G. Schäfer, B. Viel, G. P. Hellmann, M. Rehahn, M. Gallei, *ACS Appl. Mater. Interfaces* **2013**, *5*, 10623.
[36] C. E. Finlayson, P. Spahn, D. R. Snoswell, G. Yates, A. Kontogeorgos, A. I. Haines, G. P. Hellmann, J. J. Baumberg, *Adv. Mater.* **2011**, *23*, 1540.

[37] Q. Zhao, C. E. Finlayson, D. R. E. Snoswell, A. Haines, C. Schäfer, P. Spahn, G. P. Hellmann, A. V. Petukhov, L. Herrmann, P. Burdet, P. A. Midgley, S. Butler, M. Mackley, Q. Guo, J. J. Baumberg, *Nat. Commun.* **2016**, *7*, 11661.
[38] C. E. Finlayson, J. J. Baumberg, *Materials* **2017**, *10*, 688.
[39] I. B. Burgess, L. Mishchenko, B. D. Hatton, M. Kolle, M. Lončar, J. Aizenberg, *J. Am. Chem. Soc.* **2011**, *133*, 12430.
[40] H. Hu, J. Tang, H. Zhong, Z. Xi, C. Chen, Q. Chen, *Sci. Rep.* **2013**, *3*, 1484.
[41] S. Ye, Q. Fu, J. Ge, *Adv. Funct. Mater.* **2014**, *24*, 6430.
[42] P. Jiang, D. W. Smith, J. M. Ballato, S. H. Foulger, *Adv. Mater.* **2005**, *17*, 179.
[43] T. Ding, G. Cao, C. G. Schäfer, Q. Zhao, M. Gallei, S. K. Smoukov, J. J. Baumberg, *ACS Appl. Mater. Interfaces* **2015**, *7*, 13497.
[44] L. A. Wood, *J. Polym. Sci.* **1958**, *28*, 319.
[45] J. Xu, B. Chen, Q. Zhang, B. Guo, *Polymer* **2004**, *45*, 8651.
[46] C. G. Schäfer, D. A. Smolin, G. P. Hellmann, M. Gallei, *Langmuir* **2013**, *29*, 11275.
[47] Q. Zhao, C. E. Finlayson, C. G. Schaefer, P. Spahn, M. Gallei, L. Herrmann, A. V. Petukhov, J. J. Baumberg, *Adv. Opt. Mater.* **2016**, *4*, 1494.
[48] Z. Liu, F. Luo, T. Chen, *Anal. Chim. Acta* **2004**, *510*, 189.
[49] E. P. Benditt, N. Eriksen, C. Berglund, *Proc. Natl. Acad. Sci. USA* **1970**, *66*, 1044.